Soft-Switching in Capacitive-Coupled Wireless Power Transfer with *LCLC* Compensation Networks

Eli Abramov, *Student Member*, *IEEE*,
Mor Mordechai Peretz, *Member*, *IEEE*

The Center for Power Electronics and Mixed-Signal IC,
Department of Electrical and Computer Engineering
Ben-Gurion University of the Negev
P.O. Box 653, Beer-Sheva 8410501, Israel
eliab@post.bgu.ac.il, morp@bgu.ac.il
http://www.ee.bgu.ac.il/~pemic

Ilya Zeltser

Power Electronics Department
Rafael Advanced Defense Systems Ltd.
P.O. Box 2250, Haifa 31021, Israel
ilyaz@rafael.co.il
www.rafael.co.il

***Abstract*—This study details the conditions for soft-switching in capacitively-coupled resonant converters that are compensated with *LCLC* compensation networks. The comprehensive analysis revealed that by design of the compensation networks' parameters according to the highest expected coupling capacitance, zero voltage switching (ZVS) conditions are achieved over the entire operation range. The results of the analysis further outline the way to control the current at switching events, so the soft-switching is obtained for all the operating conditions while the load is resistive on the receiving side. This provides a significant potential enhancement of the power transfer and processing efficiency, in particular for applications of wireless energy where the operating frequency is very high. Prior to experimental validation, the theoretical analysis has been verified by simulations. The simulation platform incorporates a simple and flexible cross-coupled model of the capacitive medium, as well as simulation-compatible variable inductor model, which have been developed and used to evaluate the results under various conditions. To validate the theoretical framework, a custom-designed variable inductor has been realized and experiments have been carried out on a *LCLC* capacitive-based wireless power transfer (WPT) prototype operated in the MHz range, and examined at 120 mm air-gap.**

Keywords — capacitive power transfer, capacitive coupling, soft-switching, zero-voltage switching, capacitive coupler model, LCLC compensation, tuned compensation network.

I. Introduction

Over the last decade, capacitive power transfer (CPT) has been comprehensively investigated in the rapidly growing field of wireless power transfer (WPT) [1]-[6]. CPT is an attractive near-field power transfer method which overcomes some of the major limitations introduced in inductive-based WPT methods such as: undesired Eddy currents and other electromagnetic interferences (EMI). In addition, CPT systems offer design flexibility with potentially lower volume and reduced construction complexity [3]-[6]. This makes CPT technology an attractive candidate for various wireless power applications, such as biomedical implants, in-track-moving systems, various batteries charging and many more [7]-[12].

To assure better power transfer characteristics and improve the overall power transfer efficiency in capacitive WPT systems, high-frequency resonant conversion is employed, typically, in the range of several MHz. A fundamental building block of general resonant converters and in particular converters in WPT systems is a compensation network. It typically comprises a second or higher order reactance that connects and performs impedance-matching between the transmitting and receiving units. These compensation networks serve many design objectives, such as reducing circulating energy in the converter [13], lower voltage and current stresses of the switches [14]. In WPT systems, compensation networks also provide additional degrees of freedom to interact between the primary and secondary circuits and compensate for: resonant frequency, constant-voltage/current output (load-independent operation), output power and system efficiency [3], [15]-[17].

In the last few years a double-sided *LCLC* compensation network structure for CPT (Fig. 1) has been widely studied [3], [5], [6]. There, each side of the converter incorporates a T-type network, consists of *LCL* branch [6]. Combined with the parallel capacitance of the medium (or additional parallel capacitance), it results in cascaded *LC* structure. The double-sided *LCLC* configuration assures that the output power is proportional to the coupling coefficient, which is also loosely-coupled from the components' values [5], [6]. This is a significant benefit compared to other network setups employed in CPT [1]-[3]. In addition, the voltage and current stresses on the components are lower than in other methods, in particular when increasing the distance between the transmitting and receiving sides [1]-[3], [5], [6]. In spite of the considerable advantages this configuration provides, operation at high-frequencies is strongly associated with significant switching losses. Thus, to further improve the *LCLC*-based CPT systems without compromising on system's efficiency, a mechanism that assures soft-switching for wide operation range, covering all loading cases is mandatory, in particular in the context of CPT systems where the parameters dynamically vary due to changes in distance or misalignment between the transmitting and receiving sides. In [18], soft-switching analysis for double-sided *LCLC* CPT has been presented, however, only for the case of battery-oriented applications.

The objective of this study is therefore to introduce detailed analysis on the conditions for soft-switching in *LCLC* compensated resonant capacitive WPT system oriented for resistive loads at the receiving side. The analysis methodology is to explore the affecting factors on the current at the turn off instance, and consequently, outline the requirements for soft-switching at turn on and turn off. This is achieved without

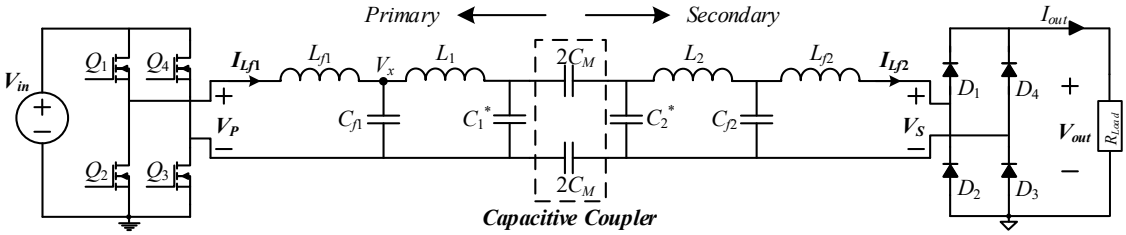

Fig. 1. Schematic diagram of a *LCLC* compensated capacitive WPT system with resistive load on the receiving side.

compromising the overall performance of the system. This study also covers simulation-compatible models of the capacitive coupler and time-continues variable inductor, that enables evaluation of the system under (and through) variations of the various parameters. It is a further objective of this study to present a practical variable inductor realization.

The rest of the paper is organized as follows: The analytical model of the *LCLC* compensated CPT system and the analysis of soft switching conditions are introduced in Section II. The description of the simulation-compatible models that have been developed for the *LCLC* WPT system are delineated in Section III, followed by a simulation case study that verifies some of system's interrelations. Section IV provides details regarding the practical implementation of the variable inductor. Experimental validation of the theoretical analysis and *LCLC* CPT prototype are provided in Section V. Section VI concludes the paper.

II. Analytical Model and Soft-Switching Analysis

A resonant capacitive *LCLC* WPT system is shown in Fig. 1. The system is driven by a full-bridge inverter (Q_1-Q_4). The load, which is represented by a resistor, R_{Load}, is fed through a diode rectifier (D_1-D_4). Both the primary and secondary side are compensated by *LCLC* resonators (L_{f1}, C_{f1}; L_1, C_1^*; L_{f2}, C_{f2}; L_2, C_2^*). The capacitive coupler in this study is implemented by two pairs of plates [2], [6]. Assuming that the two pairs are placed sufficiently far from each other, the interconnection and fringe capacitances between the pairs can be neglected. Therefore, the capacitive coupler can be represented by two series capacitors as shown in Fig. 1, there, C_M is the mutual coupling capacitance.

It has been shown in [6], that the capacitive coupler can be modeled as a two-port network, as depicted in Fig. 2a. With the aid of this two-port representation, assuming high quality factor of the input and the output filters L_{f1}, C_{f1} and L_{f2}, C_{f2}, respectively, and by applying fundamental harmonics approximation (FHA) method [19], the system can be further simplified as shown in Fig. 2b. There, V_{P1} represents the first harmonics source of the square wave V_P (Fig. 1), whereas $V_{P1}=4V_{in}/\pi$, and $Zo=8R_{Load}/\pi^2$. It should be noted that in the equivalent circuit model of Fig. 2, the capacitances C_1 and C_2 are defined as $C_1^*+C_M$ and $C_2^*+C_M$, respectively.

By applying Thevenin's Theorem to C_1 and I_1 at the input side and to C_2 and I_2 at the load side, the electrical model of the *LCLC*-based CPT system can be further modified, as shown in Fig. 3. The signals' relationships of the modified electrical model have been derived assuming that the resonant frequencies of the compensation networks' resonators at the input and at the load sides, except for L_1 and C_1, are tuned to the switching frequency, such that

$$f_r = f_{sw}\ ;\ Z_{Lf1}+Z_{Cf1}\approx 0\ ;\ Z_{Lf2}+Z_{Cf2}\approx 0\ ;\ Z_{L2}+Z_{C2}\approx 0\,, \quad (1)$$

where f_r and f_{sw} are the resonant and the switching frequencies, respectively; Z_{Cx} and Z_{Lx} are the impedances of the corresponding capacitors and inductors in Fig. 3 (x denotes the index number).

Using the relationships given in (1), and by applying Kirchhoff's voltage and current laws, the circuits in Fig. 3 can be described by the following expressions

$$\begin{cases} (2)V_x\left(\dfrac{1}{Z_{Lf1}}+\dfrac{1}{Z_{Cf1}}+\dfrac{1}{Z_{L1}}\right)=\dfrac{V_{p1}}{Z_{Lf1}}+\dfrac{V_1}{Z_{L1}} \\ (3)V_1=V_x\dfrac{Z_{C1}}{Z_{C1}+Z_{L1}}+V_2\dfrac{C_M}{C_1}\dfrac{Z_{L1}}{Z_{C1}+Z_{L1}} \\ (4)V_{x2}=V_1\dfrac{C_M}{C_2}=\dfrac{V_s}{Z_o}\left(Z_o+Z_{Lf1}\right) \\ (5)V_s=\dfrac{\left(Z_o+Z_{Lf2}\right)\|Z_{Cf2}}{\left(Z_o+Z_{Lf2}\right)\|Z_{Cf2}+Z_{L2}}\cdot\dfrac{Z_o}{Z_o+Z_{Lf2}}V_2 \end{cases}, \quad (2\text{-}5)$$

and since the resonators L_{f1}, C_{f1} and L_{f2}, C_{f2} are operated at the resonant frequency, equations (2) and (5) can be respectively simplified as follows

$$\frac{V_x-V_1}{Z_{L1}}=\frac{V_{P1}}{Z_{Lf1}}\,, \quad (6)$$

$$V_s=\frac{Z_{Cf2}Z_o}{Z_{Lf2}Z_{Cf2}+Z_{Cf2}Z_o+Z_{L2}Z_o}V_2\,, \quad (7)$$

substituting (6) into (3) yields

$$V_s=\frac{Z_{C1}}{Z_{Lf1}}V_{P1}+\frac{C_M}{C_1}V_2\,, \quad (8)$$

by rearranging (7) and (8) and after some manipulations, the secondary-to-primary voltage ratio is obtained as follows

$$\frac{V_s}{V_{P1}}=-\frac{C_{f1}}{C_m}\frac{1}{\left(\dfrac{1}{k^2}-1\right)(1+jQ)+L_{ratio}}\,, \quad (9)$$

where $k=C_M/\sqrt{C_1C_2}$ is the coupling coefficient of the capacitive coupler, $Q=Z_{Lf2}/Zo$, and $L_{ratio}=L_2/L_{f2}$. It can be observed from (9) that the voltage gain is independent of inductor L_1.

ZVS of the full-bridge switches depends on the current I_{Lf1} at the commutation instances. To obtain ZVS, two conditions have to be met. The first and the necessary one is for the current I_{Lf1} to be positive while turning off the switches Q_1 and Q_3 (the negative transition of V_P), or negative while turning off the switches Q_2 and Q_4 (the positive transition of V_P). The second is that the current magnitude at the switching instance, I_{sw}, needs to be sufficient to recharge the body capacitors of the

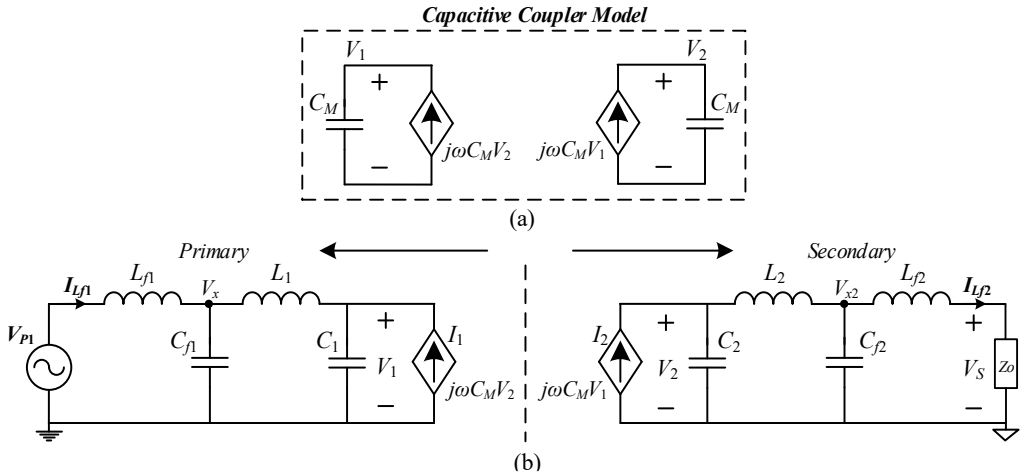

Fig. 2. (a) Two-port model of the capacitive coupler; (b) Simplified electrical model of a *LCLC* compensated CPT system by applying FHA analysis.

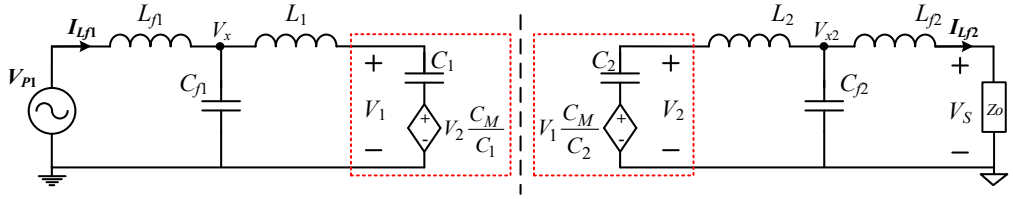

Fig. 3. Modified electrical model of a *LCLC* compensated CPT system.

switches during the switching transition. The current I_{Lf1} can be obtained from Fig. 3 as follows

$$\frac{dI_{Lf1}(t)}{dt}=\frac{V_P(t)-V_x(t)}{L_{f1}} \;;\; \begin{cases} V_P(t)=|V_{P1}|\sin(2\pi f_r t) \\ V_x(t)=|V_x|\sin(2\pi f_r t+\gamma) \\ |V_{P1}|=V_{in}\cdot \pi/4 \end{cases}, \quad (10)$$

where $|V_x|$ and γ are the magnitude and the phase of V_x, respectively.

To find V_x, first the voltage V_2 is found form the load side (see Fig. 4) by inspection

$$\begin{cases} V_2=V_1\dfrac{C_M}{C_2}\dfrac{\left(Z_o+Z_{Lf2}\right)\|\,Z_{Cf2}+Z_{L2}}{\left(Z_o+Z_{Lf2}\right)\|\,Z_{Cf2}+\underbrace{Z_{L2}+Z_{C2}}_{Z_2}} \\ f_{sw}=f_r \Rightarrow Z_2=0 \end{cases}, \quad (11)$$

then rearranging (6) and (11), and substituting them into (2) yields the following ratio

$$\frac{V_x}{V_{P1}}=\alpha\frac{C_{f1}}{C_1}\frac{(1+jQ)\left(1-k^2-1/\alpha\right)+k^2L_{ratio}}{(1+jQ)\left(1-k^2\right)+k^2L_{ratio}}, \quad (12)$$

where $\alpha=L_1/L_1^*$ is the normalized inductor's factor, and L_1^* is the normalized inductance which tunes the resonance frequency of the resonant tank L_1, C_1 to f_{sw}, i.e., $L_1=1/(2\pi\, f_{sw}C_1)$. Substituting (9) into (7) yields

$$I_{Lf1}(t)=\frac{1}{L_{f1}}\left(V_{in}\cdot\, t+\frac{|V_x|}{2\pi\cdot\, f_r}\cos(2\pi\cdot\, f_r+\gamma)-\frac{V_{in}\cdot\,\pi}{4\pi\cdot\, f_r}\right). \quad (13)$$

Finally, the current at the switching event, I_{sw}, is obtained from (13) at $t=\pi/\omega$ (half a switching period) as follows

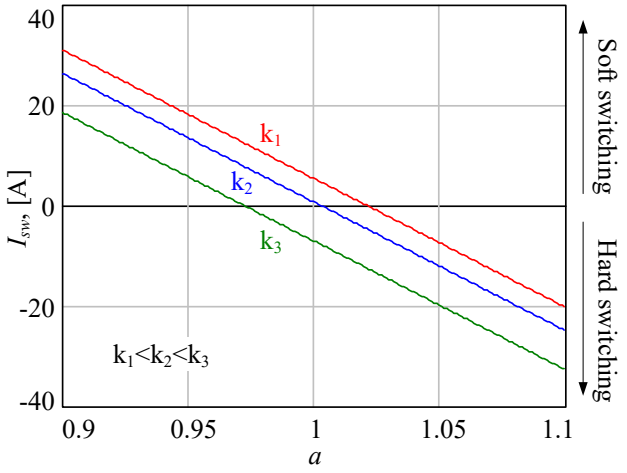

Fig. 4. Current I_{sw} as function of the normalized inductance factor α

$$I_{sw}=\frac{1}{L_{f1}}\left(\frac{V_{in}\cdot\,\pi}{2\omega}-\frac{|V_x|}{\omega}\cos\gamma\right). \quad (14)$$

Fig. 4 depicts the switching current, I_{sw}, as a function of the normalized inductance factor, α, for several coupling coefficients. For some predefined inductance value (α is constant, Fig. 4) the current I_{sw} decreases as the coupling coefficient, k, increases. This implies that if the switching current, I_{sw}, is designed to be positive for the highest expected coupling coefficient (highest C_M, smallest air-gap), soft-switching is obtained over the entire air-gaps range. However, to guarantee that the switches' body capacitors are recharged during the switching transition, I_{sw} needs to be kept high enough, regardless of variations in the input voltage and/or in the load. It can be done, as seen from Fig. 4, by changing the normalized inductance factor α. That is, if I_{sw} decreases (for

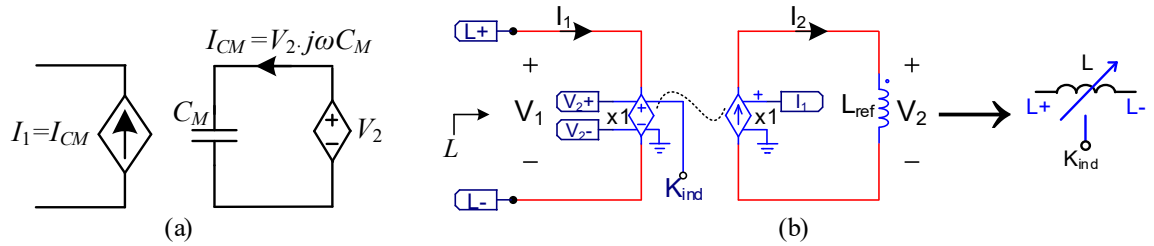

Fig. 5. Simulation-compatible models in PSIM platform: (a) Capacitive coupler; (b) Continuous-time variable inductor.

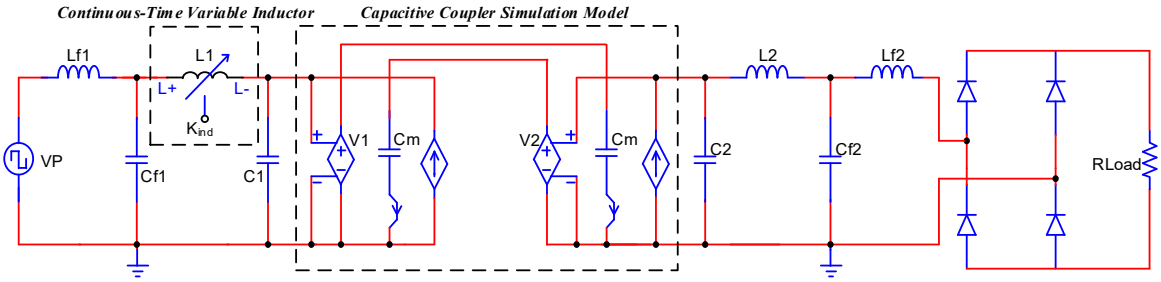

Fig. 6. Simulation-compatible model of the of the *LCLC* WPT system in PSIM platform.

example, at lower power levels operation), it can be reverted to its initial value by decreasing α (i.e. by decreasing L_1). From (13) it can be observed that changing the inductance of L_1 does not alter the input to output voltage gain, and consequently it can be controlled by a standalone control loop which does not involve the sensing of the output voltage.

III. Simulation-Compatible Models

To further investigate the implications of the coupling capacitance and L_1 on the *LCLC* CPT system behavior, the two-port network model of the capacitive coupler has been simulated using PSIM platform (PowerSim, Inc.). The capacitive voltage-dependent current source I_1 at the primary side of the coupler (Fig. 2) is generated as shown in Fig. 5a. There, an auxiliary capacitor, which emulates the coupling capacitor C_M, is exposed to the voltage V_2, and its current is replicated by voltage dependent current source to create I_1. Similarly, the capacitive voltage-dependent current source I_2 at the secondary side of the coupler (Fig. 2) is generated by replicating the current of another auxiliary coupling capacitor C_M which is exposed to the voltage V_1. In addition, to further verify the analysis and observations made in Section II, a continuous-time simulation model of a variable inductance has been designed as described in [20]. The model, illustrated in Fig. 5b, comprises dependent voltage and current sources, which emulate a non-linear transformer, loaded by some reference inductor L_{ref}. The relationship between the voltages and the currents at the transformer's terminals are defined by the following relationships

$$\begin{aligned} V_1 &= V_2 K_{ind} \\ I_2 &= I_1 \end{aligned}, \tag{15}$$

where K_{ind} is a variable transformer's ratio. From (15), the impedance of the inductor L_{ref}, reflected to the primary side, is found as follows

$$\begin{cases} Z_L = j\omega L = \dfrac{V_1}{I_1} = \dfrac{V_2 K_{ind}}{I_2} \\ Z_{Lref} = j\omega L_{ref} = \dfrac{V_2}{I_2} \end{cases} \Rightarrow Z_L = Z_{Lref} K_{ind}, \tag{16}$$

TABLE I – Adjusted Inductor L_1 Values to Obtain Soft-Switching at Constant Current for Various C_M

C_M [pF]	2	3	4	5	6	7
L_1 [µH]	60.3	60.2	60.1	59.9	59.6	59.2
I_{sw} [A] Simulation	0.2	0.2	0.2	0.2	0.2	0.2
V_{out} [V]	2.5	3.8	5.1	6.4	7.6	8.8

where Z_L is the impedance measured at the transformer's primary. Therefore, the inductor's value, reflected to the primary side is obtained to be

$$L = K_{ind} L_{ref} . \tag{17}$$

To simplify the control over the variable inductor, the inductance of L_{ref} has been set to 1 H. In this case, the effective inductance that is reflected to the primary of the transformer (terminals L+ and L- in Fig. 5b) is set by the transformer's ratio K_{ind}.

Having two-port capacitive coupler model of Fig. 5a and continuous-time behavioral model of a variable inductor (Fig. 5b), a cycle-by-cycle simulation test-bench for *LCLC* compensated capacitive WPT system has been constructed as shown in Fig. 9a. It is assumed that the coupling capacitance C_M is negligible compared to the values of C_1^* and C_2^* (see Fig. 1). The simulation model is fed from 10 V, i.e., V_P toggles between -10 and 10 V, the operating frequency is f_{sw}=1.5 MHz, and the load resistance is 10 Ω. Based on the outlines that have been established earlier in analysis section II, to guarantee ZVS conditions over the entire coupling range, L_1 is calculated to be 59.2 µH, the rest of the compensation networks' values are L_{f1}= L_{f2}=1.25 µH, C_{f1}=C_{f2}=9 nF; L_2=59.2 µH, C_1=C_2=190 pF.

The first set of simulations has been carried out by varying the coupling capacitance of the capacitive coupler from 2 pF up to 7 pF. Fig .7a shows the primary side voltage V_P, whereas the

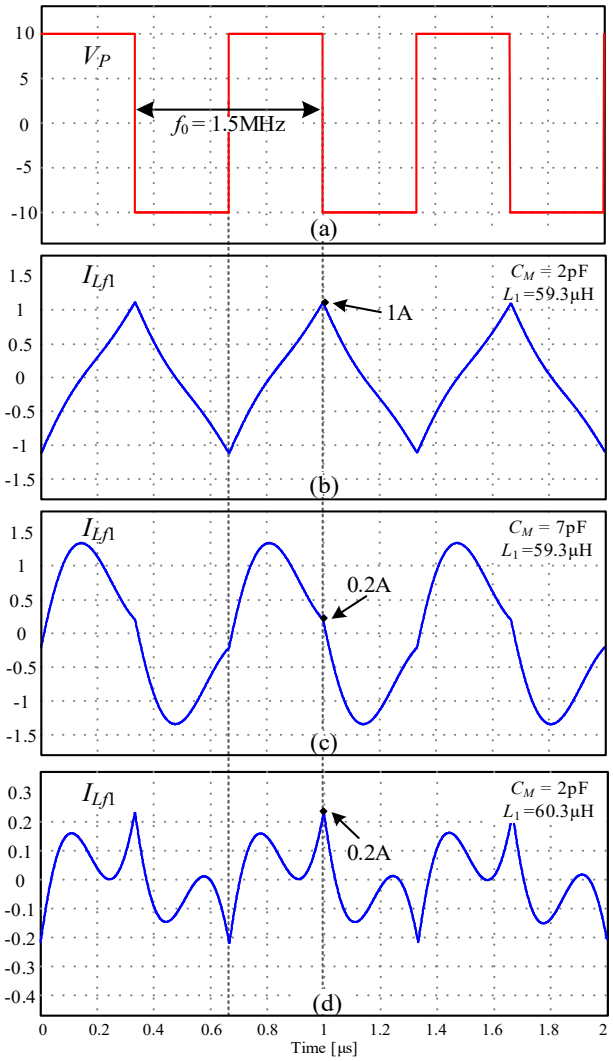

Fig. 7. Simulation waveforms of the primary side demonstrating ZVS: (a) voltage V_P, (b) current I_{Lf1} for C_M=2 pF and L_1=59.3 µH, (c) current I_{Lf1} for C_M=7 pF and L_1=59.3 µH, (d) current I_{Lf1} for C_M=2 pF and L_1=60.3 µH.

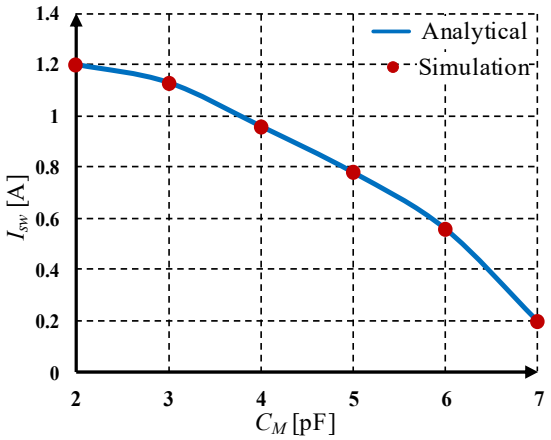

Fig. 8. The switching current, I_{sw}, as a function of the capacitive coupling (air-gap).

current I_{Lf1} for the minimum and the maximum coupling capacitances is shown in Figs. 7b and 7c, respectively It can be seen that for both cases ZVS is obtained. The current at turn off for 2 pF is 1.2 A, whereas it is 0.2 A for 7 pF. The second set

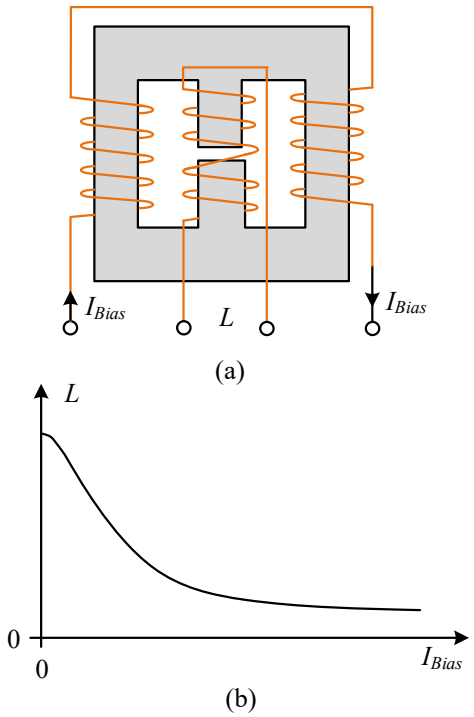

Fig. 9. (a) Variable inductor practical implementation, (b) Relationship between the inductance value and the bias current.

of measurements has been carried out while adjusting the inductor L_1 over different values of C_M to obtain a constant turn off current of I_{sw}=0.2 A. This is according to the soft-switching analysis presented in Section II. The results for these simulations are summarized in Table I. Fig. 7d shows the simulation waveform of I_{Lf1} for coupling capacitance of 2 pF while L_1 is set to 60.3 µH (see Table I).

Fig. 8 depicts the switching current, I_{sw}, as a function of the capacitive coupling C_M obtained analytically and by simulation. The simulation results verify that the switching current decreases when increasing the coupling capacitance, as predicted by the theoretical analysis.

IV. Variable Inductor Practical Implementation

A major enabler for an adaptive closed-loop operation that satisfies the conditions and criteria detailed in the previous sections, is the ability to adjust the inductance of L_1 in real-time. In this study, the implementation of variable inductor is inspired by the prior art of [21], [22]. The structure comprises an *E*-core type magnetic element with the primary inductor on the middle, gapped leg, whereas the bias/control windings are formed on the outer, non-gaped legs (Fig. 9a). If the ac component of the inductor's is small enough, so that the permeability change due to the current variations is negligibly small, the inductance value L can be estimated with the aid of several design parameters such as: number of turns n, air-gap length l_g, and the effective magnetic path length l_e. Hence, the inductance L as a function of the bias current-dependent permeability can be expressed as

$$L = \frac{n^2 \mu_0 A_e}{l_e} \frac{\mu_r(I_{Bias})}{1 + 2\frac{l_g}{l_e}\mu_r(I_{Bias})}, \qquad (18)$$

where μ_0 is the air permeability, μ_r is the magnetic core permeability, and A_e is the core area. μ_r depends on the bias current I_{Bias} and can be obtained from either the manufacturer data or by experiment [21], [23]. A simplified expression of μ_r is given by

$$\mu_r(I_{Bias}) = \frac{\mu_{mi}}{1+\left(H(I_{Bias})/H_{\text{pole}}\right)^j}, \quad (19)$$

where μ_{mi} is the permeability initial value, i.e., $\mu_{mi} = \mu_r(H=0)$, H_{pole} is the magnitude of the saturation field and j sets the permeability slope. The variable H represents magnetic field strength, which is linearly proportional to the bias current. The relationship between H and I_{Bias} is as follows

$$H(I_{Bias}) = {}^{nI_{Bias}}\!/_{l_e}. \quad (20)$$

It should be noted that the inductor's current, in the application considered in this study, has a high ac component. Consequently, the core permeability changes over the switching cycle, resulting in current distortion. However, due to the high-quality factor of the compensation networks, the high frequency components are filtered out, such that the effective inductance as a function of the bias current can be approximated as illustrated in Fig. 9b.

V. Experimental Verification

To validate and examine the theoretical predictions, an experimental *LCLC* capacitive WPT prototype has been constructed (Fig. 10a). The capacitive coupler has been designed symmetrically with four copper plates where each plate is 25x25 cm. Fig. 10b shows custom-designed variable inductor, L_1, which comprises an *E*-core type ETD49-3F3 magnetic element as discussed in detail in Section IV. All other inductors of the prototype have been constructed with a litz wire wrapped on an air-core. High-voltage multilayer SMD ceramic capacitors have been used in parallel to form the compensation capacitors. The full-bridge inverter has been realized with GaN power modules operable in several MHz [24], and the gate drive control signals for the full-bridge are generated using DE0-Nano-Altera Cyclone IV FPGA [25], at an operating frequency $f_r \approx 1.5$ MHz. The overall experimental prototype parameters and values are summarized in Table II.

The first step of the experimental validation has been carried out by characterizing the inductance of the variable inductor as a function of the bias current. Fig. 11 shows the measured results for varying the bias current in the range of 0.3 to 0.5 A, which provides 1.5X inductance variation, covering the required tuning range, as summarized in Table I. It should be noted that to obtain the desired inductance for L_1 throughout the experiments, I_{Bias} has been manually regulated by a power supply.

TABLE II – Experimental Prototype Specifications and Parameters

Parameter	*Design Value*
Input voltage V_{in}	10 V
Coupling plates	25x25 cm
Full-bridge transistors	LMG5200
Operating frequency f_r	1.5 MHz
Load resistance R_{Load}	10 Ω
Lf_1 , Lf_2	1.25 µH
L_1 , L_2	40-62 µH, 60 µH

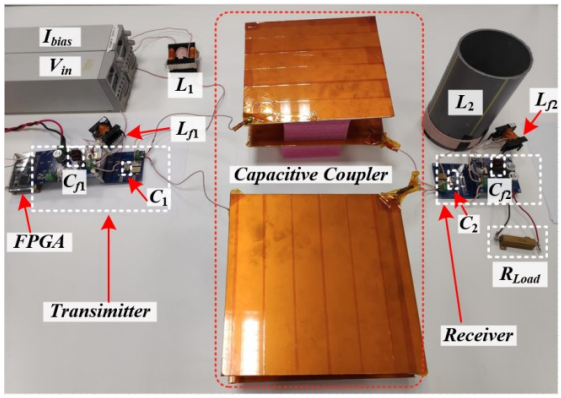

(a)

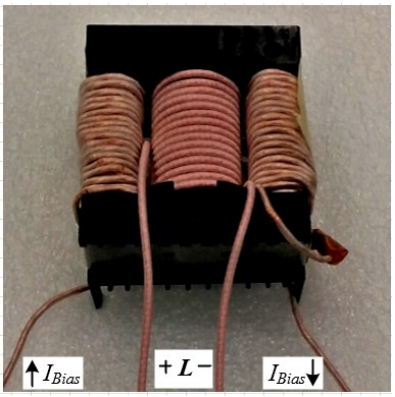

(b)

Fig. 10. (a) Experimental setup of a *LCLC* compensated capacitive WPT prototype, (b) Zoom-in on the E-core type based variable inductor.

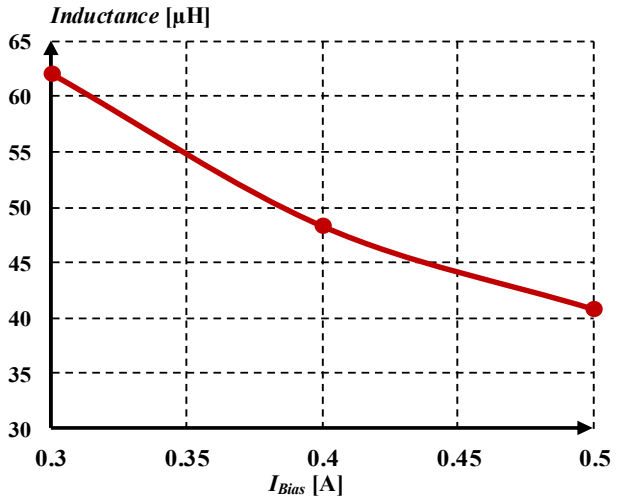

Fig. 11. Inductance of the variable inductor L_1 as a function of the bias current.

Next, the inductor L_1 has been adjusted to satisfy ZVS conditions over the entire coupling range, that is, adjusting L_1 according to the highest C_M (7 pF). Fig. 12 shows experimental waveforms of the primary side voltage V_P and current I_{Lf1} for two different coupling capacitances (2 pF and 7 pF). As can be observed, for both cases ZVS is obtained. The conditions for 2 pF the current at turn off is 1 A, whereas it is 0.2 A for 7 pF. To

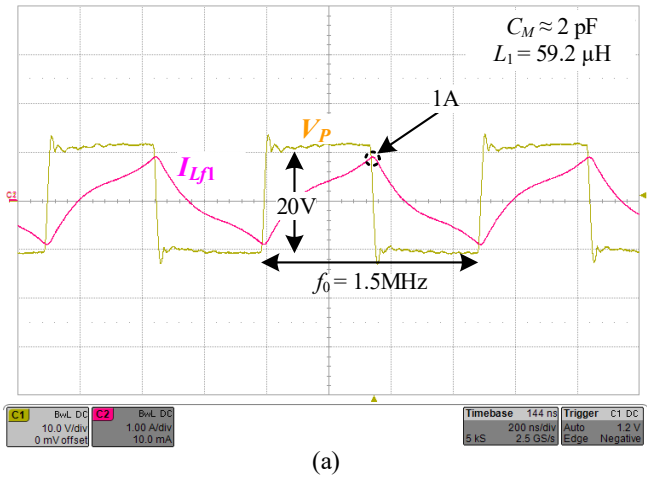

(a)

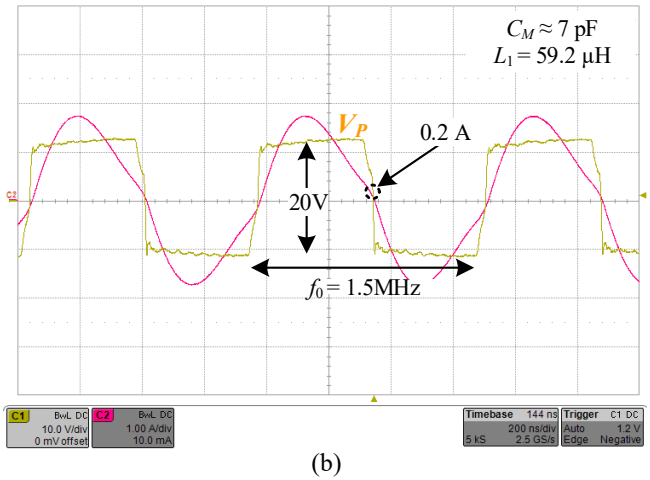

(b)

Fig. 12. Experimental waveforms of the primary side voltage V_P (yellow curve – 10V/div) and current I_{Lf1} (pink curve – 1A/div) for L_1 =59.2 µH: (a) C_M ≈2 pF, (b) C_M≈7 pF and. Time scale 200ns/div.

further validate the soft-switching analysis, by adjusting the inductor L_1 according to the relationships given in (14), the current at turn off has been calibrated to be in the vicinity of 0.2- A over the entire coupling operating range. The resulting inductor L_1 values for the entire given C_M range are as summarized in Table I. Fig. 13 depicts experimental waveforms of the primary for C_M ≈2 pF while L_1 =60.3 µH. As can be observed the soft-switching conditions are satisfied such that the current at turn off I_{sw} ≈ 0.2 A. The experimental results tightly follow the results obtained by the simulations in Section III as well as the theoretical predictions.

VI. Conclusion

Detailed soft-switching analysis of a *LCLC*-compensated resonant-based CPT systems with resistive loads has been presented. Based on the comprehensive analysis, it has been established that ZVS is achieved over the entire operating range if the system's parameters are designed for the highest expected coupling capacitor. It follows from the analysis presented in this study, that the current at turn off can be controlled for various operating conditions by altering the inductance of the primary compensation network. This way, sufficient energy to recharge

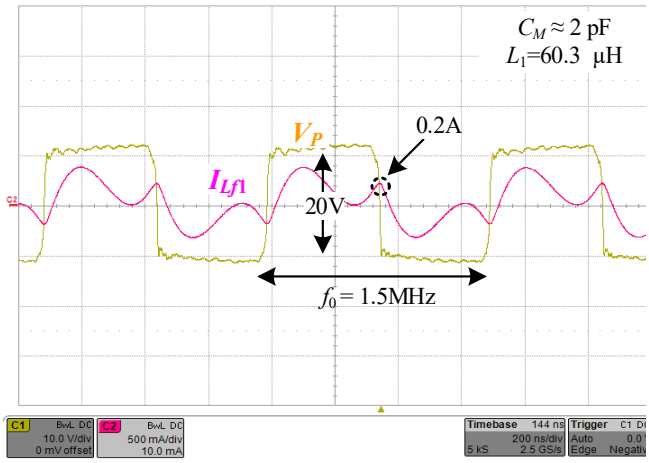

Fig. 13. Experimental waveforms of the primary side voltage V_P (yellow curve – 10V/div) and current I_{Lf1} (pink curve – current scale 0.5A/div) for C_M ≈2 pF and L_1=60.3 µH. Time scale 200ns/div.

the switches' body capacitances is obtained over the entire operating range further reducing the switching losses. This technique can be of a particular importance in high frequency *LCLC* WPT systems with very fast rise and fall times, where substantial current is required to recharge the capacitors rapidly. It is further shown that controlling the current at the switching instance by the method presented in this study does not affect the voltage gain ratio, therefore, the inductance can be controlled by means of an independent control loop, with no sensing of the output voltage, which significantly simplifies the overall WPT system. An excellent agreement has been found between the theoretical predictions, simulations and experimental results.

Acknowledgement

This research was supported by the ISRAEL SCIENCE FOUNDATION grant number 2186/19.

This research was also supported by The Prof. A. Pazy Research Foundation.

References

[1] F. Lu, H. Zhang, H. Hofmann, C. Mi, "A loosely coupled capacitive power transfer system with LC compensation circuit topology," *Proc. IEEE Energy Convers. Congr. Expo. (ECCE)*, pp. 1-5, 2016.

[2] F. Lu, H. Zhang, C. Mi, "A two-plate capacitive wireless power transfer system for electric vehicle charging Applications," *IEEE Trans. Power Electron*, vol. 33, no. 2, pp. 946-969, Aug. 2017.

[3] F. Lu, H. Zhang, H. Hofmann, and C. Mi, "A double-sided LC compensation circuit for loosely-coupled capacitive power transfer," *IEEE Trans. Power Electron*., vol. 33, no. 2, pp. 1633 – 1643, Feb. 2017.

[4] M. P. Theodoridis, "Effective capacitive power transfer," *IEEE Trans. Power Electron*., vol. 27, no. 12, pp. 4906–4913, Dec. 2012.

[5] F. Lu, H. Zhang, H. Hofmann, and C. Mi, "A double-sided *LCLC* compensated capacitive power transfer system for electric vehicle charging," *IEEE Trans. Power Electron.*, vol. 30, no. 11, pp. 6011–6014, Jun. 2015.

[6] H. Zhang, F. Lu, H. Hofmann, W. Liu, and C. C. Mi, "A four-plate compact capacitive coupler design and LCL-compensated topology for capacitive power transfer in electric vehicle charging

application," *IEEE Trans. Power Electron*., vol. 31, no. 12, pp. 8541–8551, Dec. 2016.
[7] A. M. Sodagar and P. Amiri, "Capacitive coupling for power and data telemetry to implantable biomedical microsystems," in *Proc. 4th Int. IEEE/EMBS Conf. Neural Eng.*, Apr. 29–May 2, 2009, pp. 411–414.
[8] Liu. Chao, A. P. Hu, and M. Budhia, "A generalized coupling model for capacitive power transfer systems," in *Proc. 36th Annu. Conf. IEEE Ind. Electron. Soc*., Nov.7–10, 2010, pp. 274–279.
[9] S. Li and C. Mi, "Wireless Power Transfer for Electric Vehicle Applications," *IEEE Journal of Emerging and Selected Topics in Power Electronics*, vol. PP, pp. 1-1, 2014.
[10] S. Jaegue et al., "Design and implementation of shaped magnetic resonance-based wireless power transfer system for roadway-powered moving electric vehicles," *IEEE Trans. Ind. Electron*., vol. 61, no. 3, pp. 1179–1192, Mar. 2014.
[11] S.Y.R. Hui, W. Zhong and C.K. Lee, "A critical review of recent progress in mid-range wireless power transfer," *IEEE Transactions on Power Electronics*, vol. 29, no. 9, pp. 4500-4511, September 2014.
[12] F. Musavi and W. Eberle, "Overview of wireless power transfer technologies for electric vehicle battery charging," *IET Power Electronics*, vol. 7, no. 1, pp. 60–66, 2014.
[13] C. Lin and F. Lee, "Design of a piezoelectric transformer converter and its matching networks," *Proc. IEEE-PESC'94 Conf.*, vol. 1, pp. 607–612, 1994.
[14] M. Evzelman and M. M Peretz "Optimal design of a class-E resonant driver," *IET Power Electronics,* vol. 8, no.8, pp 1552-1557, Apr. 2015.
[15] W. Zhang and C. Mi, "Compensation topologies for high power wireless power transfer systems," *IEEE Transactions on Vehicular Technology*, vol. 65, no.6, pp. 4768-4778, July 2015.
[16] S. Sinha, A. Kumar, S. Pervaiz, B. Regensburger and K.K. Afridi, "Design of efficient matching networks for capacitive wireless power transfer systems," *Proceedings of the IEEE Workshop on Control and Modeling for Power Electronics (COMPEL)*, Trondheim, Norway, June 2016.
[17] A. Kumar, S. Sinha, A. Sepahvand, K. K. Afridi, "Improved design optimization for high-efficiency matching networks," *IEEE Transactions on Power Electronics*, vol. 33, no. 1, pp. 37-50, Jan 2018.
[18] E. Abramov, I. Zeltser, and M. M. Peretz, "Soft-switching and efficient power transfer in capacitive wireless systems with LCLC compensation networks," in *IEEE Proc. International Conference on Power Electronics and ECCE Asia (ICPE 2019-ECCE Asia)*, pp. 979-985, 2019.
[19] R. L. Steigerwald, "A comparison of half-bridge resonant converter topologies," *IEEE Transactions on Power Electronics*, vol. 3, no. 2, pp. 174-182, April 1988.
[20] S. Ben-Yaakov, M. M. Peretz, "Simulation bits: a SPICE behavioral model of non-linear inductors," *IEEE Power Electronics Society Newsletter*, Fourth Quarter, pp. 9-10, 2003.
[21] S. Ben-Yaakov and M. M. Peretz, "A self-adjusting sinusoidal power source suitable for driving capacitive loads," *IEEE Trans. Power Electron.*, vol. 21, no. 4, pp. 890–898, Jul. 2006.
[22] S. S. Ahsanuzzaman, T. McRae, M. M. Peretz, and A. Prodic, "Low volume buck converter with adaptive inductor core biasing," in *Proc. IEEE Appl. Power Electron. Conf. Expo. (APEC)*, Feb. 2012, pp. 335–339.
[23] O. Ezra and M. M. Peretz, "Magneto-electro-mechanical modeling of magnetic actuation systems," in *Proc. IEEE Applied Power Electronics Conference and Exposition (APEC),* 2015, pp. 2628–2634.
[24] Texas Instrument: 'LMG5200 80-V, 10-A GaN Half-Bridge Power Stage' available at: http://www.ti.com/lit/ds/symlink/lmg5200.pdf, accessed March 2017.
[25] DE0-Nano Development and Education Board user manual, terasIC Inc. - Intel, 2016.